Phase equilibrium modelling of the amphibolite to granulite facies transition in metabasic rocks (Ivrea Zone, NW Italy)

Short Title:

Amphibolite–granulite transition, Ivrea Zone

Barbara E. Kunz[a*] and Richard W. White[b]

[a] *School of Environment Earth and Ecosystems Sciences, The Open University, Walton Hall, Milton Keynes MK7 6A, UK*

[b] *School of Earth & Environmental Sciences, University of St Andrews, KY16 9AL Scotland, UK*

*Corresponding author e-mail address: barbara.kunz@open.ac.uk (B.E. Kunz).

Phase equilibrium modelling of the amphibolite to granulite facies transition in metabasic rocks (Ivrea Zone, NW Italy)

Barbara E. Kunz[a*] and Richard W. White[b]

[a] *School of Environment Earth and Ecosystems Sciences, The Open University, Walton Hall, Milton Keynes MK7 6A, UK*

[b] *School of Earth & Environmental Sciences, University of St Andrews, KY16 9AL Scotland, UK*

This article has been accepted for publication and undergone full peer review but has not been through the copyediting, typesetting, pagination and proofreading process, which may lead to differences between this version and the Version of Record. Please cite this article as doi: 10.1111/jmg.12478

*Corresponding author e-mail address: barbara.kunz@open.ac.uk (B.E. Kunz).

ABSTRACT

The development of thermodynamic models for tonalitic melt and the updated clinopyroxene and amphibole models now allow the use of phase equilibrium modelling to estimate *P*–*T* conditions and melt production for anatectic mafic and intermediate rock types at high-temperature conditions.

The Permian mid-lower crustal section of the Ivrea Zone preserves a metamorphic field gradient from mid amphibolite facies to granulite facies, and thus records the onset of partial melting in metabasic rocks. Interlayered metabasic and metapelitic rocks allows the direct comparison of *P*–*T* estimates and partial melting between both rock types with the same metamorphic evolution. Pseudosections for metabasic compositions calculated in the Na_2O–CaO–K_2O–FeO–MgO–Al_2O_3–SiO_2–H_2O–TiO_2–O (NCKFMASHTO) system are presented and compared with those of metapelitic rocks calculated with consistent endmember data and *a*–*x* models. The results presented in this study show that *P*–*T* conditions obtained by phase equilibria modelling of both metabasic and metapelitic rocks give consistent results within uncertainties, allowing integration of results obtained for both rock types. In combination, the calculations for both metabasic and metapelitic rocks allows an updated and more precisely constrained metamorphic field gradient for Val Strona di Omegna to be defined. The new field gradient has a slightly lower d*P*/d*T* which is in better agreement with the onset of crustal thinning of the Adriatic margin during the Permian inferred in recent studies.

Keywords: metabasic rocks, Ivrea Zone, mineral equilibria modelling, partial melting, THERMOCALC

1 INTRODUCTION

Understanding the *P*–*T*, melt production and melt loss evolution of high-temperature terranes is crucial to comprehending crustal evolution during orogenesis as melting and melt loss are the main driving forces of crustal differentiation (e.g., Brown & Rushmer, 2006; Johnson, Fischer, White, Brown, & Rollinson, 2012).

Regional metamorphic belts which expose continuous crustal sections represent ideal areas to study melting processes over a range of *P*–*T* conditions (e.g. Binns, 1964; Greenfield, Clarke, & White, 1998; Johnson, Kirkland, Reddy, & Fischer, 2015; Redler, White, & Johnson, 2013; Sawyer, 1991; Waters, 1986; White, Powell, & Clarke, 2003), allowing us to test and validate our observations and models derived through experimental petrology or geophysical observation (White et al., 2003).

A significant proportion of the lower continental crust is inferred to be made up of basic rocks (e.g. Rudnick & Fountain, 1995). Under high-temperature metamorphic conditions (> 800°C, Rushmer, 1991; Wyllie & Wolf, 1993) these rocks can partially melt, evidenced by migmatites in metamorphic terranes (e.g. Hartel & Pattison, 1996; Johnson et al., 2012; Sawyer, 1991). Combining phase equilibrium modelling with field observation of migmatites has proven to be a powerful tool to study the metamorphic evolution of high-temperature terranes (e.g. Johnson & Brown, 2004; Johnson & White, 2011; Korhonen, Saito, Brown, & Siddoway, 2010; White et al., 2003; White, Powell, & Halpin, 2004; White, Pomroy, & Powell, 2005). In recent years, the development and refinement of *a*–*x* models for rocks of mafic composition (Dale, Powell, White, Elmer, & Holland, 2005; Diener, Powell, White, & Holland, 2007; Diener & Powell, 2012; Green, Holland, & Powell, 2007; Green et al., 2016) and their use in determining *P*–*T* conditions, melt composition and production of metamorphic rocks have increased our understanding of melting and metamorphic evolution of mid-lower crustal rocks (e.g., Chapman, Clarke, Piazolo, & Daczko, 2017; Feisel, White, Palin, & Johnson, 2018; Palin et al., 2016; White, Palin, & Green, 2017; Yakymchuk, 2017).

The new activity–composition relationships for minerals and melt in Green et al. (2016) allow high-temperature suprasolidus equilibria in metabasic rocks to be calculated for the first time. This study uses THERMOCALC (Powell & Holland, 1988) and the new suite of models for mafic rocks from Green et al. (2016) to test the comparability of phase equilibrium modelling on metabasic rocks with those made on metapelitic rocks. Being able to compare the results with each other is crucial when linking *P*–*T* constraints across the different chemical systems and common rock types. Being able to extract reliable *P*–*T* conditions from metabasic rocks that may be directly compared to those from other rock types is especially important in terranes where no or few metapelitic rocks exist, such is the case in many Archean terrains (e.g. Palin, White, & Green, 2016; White et al., 2017).

The Ivrea Zone (NW Italy; Figure 1) is a well-studied profile through the mid to lower continental crust which exposes a continuous metamorphic field gradient through a sequence of interlayered metapelitic and metabasic rocks. Metamorphic conditions range from mid amphibolite facies (~650°C) to granulite facies (>900°C) conditions, covering the onset of partial melting in both metabasic and metapelitic rocks. Many previous studies have investigated the *P–T* conditions, partial melting and melt loss of the metapelitic rocks (Ewing, Hermann, & Rubatto, 2013; Henk, Franz, Teufel, & Oncken, 1997; Luvizotto & Zack, 2009; Redler, Johnson, White, & Kunz, 2012; Redler et al., 2013; Schmid & Wood, 1976; Zingg, 1980). Despite their potential to help constrain the metamorphic conditions of the Ivrea Zone, to date, the extraction of *P–T* conditions from metabasic rocks of the Kinzigite Formation have been restricted to only a few conventional thermobarometry studies (Henk et al., 1997; Reinsch, 1973a, b).

Here, we present *P–T* pseudosections for six metabasic rocks from Val Strona di Omegna to constrain the *P–T* conditions of metamorphism and melt productivity. The results from the metabasic rocks are then compared to the samples used in the study by Redler et al. (2012), which have been recalculated with the updated Holland and Powell (2011) dataset to allow direct comparison with the metabasic rocks. The results from metabasic and metapelitic rocks are in good agreement with each other, suggesting information may be combined from both rock types to better constrain metamorphic conditions. Furthermore, the combined results provide a refined version of the metamorphic field gradient proposed by Redler et al. (2012).

2 GEOLOGICAL SETTING

The Ivrea Zone in the Southern Alps (N-Italy) exposes a NW dipping and NE–SW striking tilted cross section through the Permian mid to lower continental crust of the Adriatic margin (e.g., Handy, Franz, Heller, Janott, & Zurbriggen, 1999; Zingg, Handy, Hunziker, & Schmid, 1990). In the NW the Ivrea Zone is bordered by the Insubric Line (Gansser, 1968; Schmid, Zingg, & Handy, 1987) separating it from the units of the Central and Western Alps. Towards the SE the Cossato-Mergozzo-Brissago Line (CMB Line) and Pogallo Line separate the Ivrea Zone from the upper crustal units of the Serie dei Laghi/Strona-Ceneri Zone (Boriani, Burlini, & Sacchi, 1990; Handy, 1987; Mulch, Rosenau, & Doerr, 2002; Mulch, Cosca, & Handy, 2002).

The Ivrea Zone (Figure 1) can be subdivided into magmatic rocks (Mafic Complex), metamorphic rocks (Kinzigite Formation) and subordinate ultramafic rocks (e.g., Quick et al., 2003; Zingg, 1978). The Mafic Complex intruded during the Permian (288 ± 4 Ma; Peressini, Quick, Sinigoi, Hofmann, & Fanning, 2007) into the Kinzigite Formation (Sinigoi, Quick, Demarchi, & Klötzli, 2011). In Val Sesia the Mafic Complex reaches its maximum thickness with ~8 km, exposing a layered intrusive series with dominantly amphibole gabbro's towards the base and mostly gabbro's, diorites and granites towards the top (Sinigoi, Quick, Mayer, & Budahn, 1996). Between the lower and upper Mafic Complex the 'paragneiss-bearing belt' is an area were strongly restitic septa of Kinzigite Formation paragneisses crop out in thin slices (Sinigoi et al., 1991; Quick, Sinigoi, Negrini, Demarchi, & Mayer, 1992).

The Kinzigite Formation consists of interlayered metasedimentary and metabasic rocks (e.g., Bertolani, 1968; Zingg, 1978). The original relationship between the different rock types is unclear due to the strong metamorphic overprint and deformation during the Permian (e.g., Schmid, 1993; Vavra, Schmid, & Gebauer, 1999). In Val Strona di Omegna (Figure 2) a continuous section from mid amphibolite to granulite facies conditions is exposed along 14 km of river section (e.g., Henk et al., 1997; Kunz, Johnson, White, & Redler, 2014; Redler et al., 2012; Schmid, 1993; Zingg, 1978). Despite the occurrence of high-temperature shear zones in the area of the amphibolite to granulite facies transition (Rosarolo shear zone) a near-continuous metamorphic field gradient (Redler et al., 2012) and continuous geochronological results (e.g. Henk et al., 1997; Siegesmund et al., 2008) have been reported. Suggesting the offset or shortening within these shear zones is within the uncertainty of the thermobaromentric and geochronological methods used. The *P*–*T* conditions inferred for Val Strona di Omegna, using phase equilibrium modelling and Zr-in-rutile thermometry on metapelitic rocks, record peak metamorphic conditions of >900°C and 10–12 kbar (Ewing et al., 2013; Luvizotto & Zack, 2009; Redler et al., 2012, 2013). Compared to the many studies on metapelitic rocks and igneous rocks from the Mafic Complex, only few studies have looked extensively into the metamorphic and geochemical evolution of the metabasic rocks in Val Strona di Omegna (Bea & Montero, 1999; Kunz et al., 2014; Reinsch, 1973a, b; Sills & Tarney, 1984). Based on trace element patterns Sills and Tarney (1984) classified the metabasic rock in Val Strona di Omegna as N-MORB and E-MORB with a possible accretionary wedge origin for the section.

Similar to other granulite facies terranes (Harley, 2016; Kelsey & Hand, 2015) the ages obtained for the high-temperature granulite facies metamorphism in the Ivrea Zone span a range of more than 50 million years. A first phase of high-temperature conditions has been dated to 316 ± 3 Ma (Ewing et al., 2013), followed by a potentially extended period of high-temperature conditions until *c.*260 Ma (Ewing et al., 2013; Kunz, Regis, & Engi, 2018; Vavra et al., 1999).

Studies from Barboza, Bergantz and Brown (1999), Barboza and Bergantz (2000), Redler et al. (2012) presented convincing evidence that the Mafic Complex was not the primary heat source for the regional granulite facies metamorphism in the Kinzigite Formation and that the high-grade metamorphism preceded intrusion. However in Val Sesia (Figure 1) a local contact aureole of 1–3 km at the contact to the mafic intrusion can be observed (Barboza et al., 1999; Redler et al., 2012) where the Mafic Complex intrudes rocks that reached only amphibolite facies regional metamorphic conditions.

3 FIELD AND PETROGRAPHIC OBSERVATIONS

In Val Strona di Omegna, where the continuous metamorphic field gradient is best exposed, metabasic rocks crop out as elongated lenses between metapelitic rocks and minor metapsammites, calcsilicates, marbles and ultramafic rocks (Bertolani, 1968). A detailed description of the field and petrographic features of metabasic rocks from Val Strona di Omegna is given in Kunz et al. (2014). In this study, six samples (Figure 2 and Table 1) from the study of Kunz et al. (2014) were selected for phase equilibrium modelling and are briefly described below. In the present study migmatite terminology by Sawyer (2008) is used and mineral abbreviations are those used by THERMOCALC.

The mid amphibolite facies samples are commonly massive to weakly-foliated fine-grained amphibolites (Figure 3a), locally with rare cm-sized porphyroblasts of green hornblende. The metabasic rocks crop out as elongate lenses with a width of 10 cm to ~100 m. Evidence for partial melting, such as coarse grained leucocratic segregation (leucosome) are not observed in the field at this grade. However thin films of quartz along grain boundaries (Figure 4a) could be evidence for partial melting. Quartz and less commonly calcite veins cross-cut the mid amphibolite facies metabasic rocks (Figure 3a). The samples typically have a mineral assemblage of (green) hornblende, plagioclase, quartz, biotite and ilmenite (Table 1 and Figure 4a). Intergrowths of hornblende and biotite are common (Figure 4a) and in places define a weak foliation.

In the part of Val Strona di Omegna from Marmo to Rosarolo rocks of upper amphibolite facies conditions are exposed (Figure 2). In this part of the valley, metabasic rocks are more abundant than in others. The metabasic rocks start to show layering of leucocratic and melanocratic minerals (Figure 3b). For most of the upper amphibolite facies macroscopically it remains unclear if this is caused by *in situ* partial melting or subsolidus differentiation. Just south of the village of Rosarolo the metabasic rocks become more granoblastic and show the first macroscopic evidence for partial melting (Figure 3c), such as segregation of leucocratic material with peritectic clinopyroxene (Figure 3c). At first the leucocratic patches macroscopic visible in the field are a maximum a few cm big and discrete from each other (Figure 5a). Within several hundred metres towards the granulite facies transition the leucosome start to occur in the form of veins, both parallel to the foliation as well as cross cutting the foliation. The mineral assemblage (Table 1 and Figure 4b, c) of the metabasic rocks in the upper amphibolite facies is (green/brown) hornblende, clinopyroxene, plagioclase, biotite, quartz and ilmenite. Hornblende occurs as prograde matrix grains, as inclusions in clinopyroxene as well as retrograde partial replacement of clinopyroxene (Figures 3c and 4c, e). In thin section, features typical for partial melting such as thin films of quatzofeldspathic minerals along grain boundaries can be observed (Figure 4b, c).

Metabasic rocks from the granulite facies show extensive field evidence for partial melting such as *in situ* nebulitic to stromatic leucosomes (Figures 3d–f and 5b). Interconnected leucosome vein networks and former melt pools (i.e. located in boudin necks) commonly host coarse-grained clinopyroxene (Figures 3d–f and 4e, f). Leucosome veins can be up to a metre wide and, where exposure allows, can be followed for several meters. No clear pattern of cross-cutting relationships between leucosomes derived from metapelitic and metabasic rocks can be found in outcrops where both rock types are present. The main mineral assemblage of granulite facies metabasic rocks is clinopyroxene, orthopyroxene, (brown) hornblende, plagioclase, biotite, garnet, ilmenite and quartz (Table 1 and Figure 4d–f). Clinopyroxene, orthopyroxene and garnet commonly form cm-sized porphyroblasts. In the highest grade samples (IZ 100) hornblende is only present as relics or secondary replacement (Figure 4f).

4 PHASE EQUILIBRIUM MODELLING

For pseudosection modelling the program THERMOCALC 3.45i (Powell & Holland, 1988) together with the internally consistent thermodynamic dataset of Holland and Powell (2011), ds63 (created 24 Jan, 2015) for metabasic and ds62 (created 6 Feb, 2012) for metapelitic rocks has been used. The differences between these two versions of the Holland and Powell (2011) dataset are relatively minor and do not drastically influence the comparability of the two sets of calculations. The calculations were undertaken in the system NCKFMASHTO (Na_2O–CaO–K_2O–FeO–MgO–SiO_2–H_2O–TiO_2–O). The following *a–x* models were used: tonalitic melt, clinoamphibole, clinopyroxene-augite (Green et al., 2016), orthopyroxene, garnet, biotite (White, Powell, Holland, Johnson, & Green, 2014), epidote (Holland & Powell, 2011), feldspars (Holland & Powell, 2003), magnetite (White, Powell, & Clarke, 2002) and ilmenite (White, Powell, & Holland, 2001). The same *a–x* models were used for the metapelite calculations with the exception that the white mica model and the haplogranitic melt model of White et al. (2014) were used. Additional pure phases for pseudosection calculation are quartz, rutile, titanite, sillimanite and aqueous fluid (H_2O).

The *P–T* pseudosections calculated for the metabasite samples are given in Figure 6. For pseudosection calculations normalised bulk rock composition in mol.% from XRF major element measurements were used (compositions are given above each pseudosection and Table 2). Loss on ignition (LOI) was utilized to determine the maximum potential amount of H_2O in the bulk rock. This assumption leads to uncertainties, since SO_3, CO_2 and other fluids can influence the LOI significantly. Fe_2O_3 values were determined by iron titration. Manganese was not considered in the calculations, but is unlikely to have a strong effect on the results at mid amphibolite to granulite facies conditions, akin to that in metapelitic rocks (White et al., 2014). Each pseudosection shows the inferred peak mineral assemblage field highlighted and with bold text. Figure 7a shows a compilation of these peak assemblage fields from each sample presenting the metamorphic field gradient preserved in the metabasic rocks from Val Strona di Omegna. The black bold line in each pseudosection represents the solidus, the dashed line marks the hornblende out reaction. The thin white dashed lines in the pseudosection IZ 006 and IZ 014b are normalised mol.% contours for melt. Mineral abbreviations used in the *P–T* pseudosections are the following; L – tonalitic melt, hb – hornblende, aug – augite (clinopyroxene), opx – orthopyroxene, g – garnet, pl – plagioclase, mt – magnetite, ilm –ilmenite, ep – epidote, bi – biotite, sph – titanite, ru – rutile, q – quartz, H_2O – fluid phase.

4.1 Mid amphibolite facies samples

Both metabasic samples IZ 006 and IZ 014b from the mid amphibolite facies have the peak assemblage hb–pl–bi–ilm–q±L (Figure 6a, b). No field evidence for partial melting was observed in these samples, however the presence of intergranular quartz and feldspar with low apparent dihedral angles (Figure 4a) observed in thin section is consistent with the presence of melt. This translates to suprasolidus *P–T* conditions for IZ 006 of 680–770°C at 3–7.6 kbar in IZ 006 and 700–800°C at 3–9 kbar in IZ 014b (Table 1). Given the limited amount of partial melting evidence in thin section, the rocks are likely to be just above the solidus. The solidus in both mid amphibolite facies pseudosections occurs between 650 and 750°C, while the hb-out reaction in sample IZ 006 occurs between ~820–930°C and in sample IZ 014b above 950°C.

4.2 Upper amphibolite facies samples

The two samples (IZ 035 and IV 051) from the upper amphibolite facies have narrow peak assemblage fields with the mineral assemblage hb–aug–pl–ilm–q–L (Figure 6c, d). This assemblage is indicative of the samples having experienced *P–T* conditions of 830–850°C at 7.2–8.5 kbar and 840–860°C at 6.7–8.5 kbar respectively (Table 1). For both samples the H_2O content measured by LOI needed to be increased to calculate a pseudosection containing the peak mineral assemblage observed in the rock. This was done by calculating *T–x* diagrams for H_2O at 7 kbar and then using the rbi function in THERMOCALC to infer the H_2O content for the peak mineral assemblage (*T–x* diagrams are provided in Figure S3). Compared to the mid amphibolite facies samples a shift in the solidus (bold line) towards higher temperatures between 750–850°C can be observed. The hornblende-out (dashed line) reaction in the two upper amphibolite facies samples occurs at similar conditions as in sample IZ 014b above 950°C.

4.3 Granulite facies samples

The granulite facies, the metabasic samples have inferred peak assemblage hb–aug–opx–g–pl–ilm–L ± q (Figure 6e, f). The assemblage field in the pseudosections give *P–T* estimates over a wide range of temperature conditions from 850–1050°C (IZ 161) and 940–990°C (IZ 100) over a limited pressure range of 7.2–9.5 kbar and 7.3–9.8 kbar respectively (Table 1). Both granulite facies samples show a solidus (bold line) shifted towards

higher temperatures >800–850°C compared to (hydrated) mid amphibolite facies samples (solidus ~650–750°C). This is in agreement with the observed low H_2O content (0.51–0.07 wt%) for granulite facies samples and likely the result of melt loss at high-grade conditions. Similarly to the lower grade samples, the hb-out reaction (dashed line) in IZ 161 occurs above 950°C, while in sample IZ 100 it occurs at 900–950°C.

4.4 Metamorphic field gradient and comparison with metapelite results

In addition to the pseudosections calculated for the six metabasic samples, the peak assemblage field for the metapelitic samples from the same valley transect studied by Redler et al. (2012, 2013) have been recalculated with the new dataset ds62 (Figure 7b). The recalculation was necessary to account for changes in the *P–T* position of the peak assemblage fields using the new dataset and *a–x* models compared to the older ds55 set used by Redler et al. (2012, 2013). This allows a direct comparison between the pseudosection calculations and the *P–T* conditions obtained for the two rock types (Figure 7b). For a detailed discussion on the differences between ds62 and previous datasets see Holland and Powell (2011). The new metamorphic field gradient presented in Figure 7b shows an overlap in the peak mineral assemblage fields between the results from metapelitic rocks and those from metabasic rocks. Furthermore, the difference between the previous presented metamorphic field gradient (Redler et al., 2012) with the results presented here are clear in Figure 7b. Applying the new internally consistent thermodynamic dataset (ds6) and associated *a–x* models to both rock types shifts the inferred mineral assemblage fields to lower pressures, particularly at higher *T*, creating a field gradient with a lower dP/dT (≈0.013 kbar/°C) than that presented in Redler et al. (2012) ≈0.024 kbar/°C.

4.5 Melt production and composition

Metamorphic field gradients through a sequence of rocks provide a unique opportunity to see the evolution of a given rock type at different metamorphic grades. This is of particular use in suprasolidus systems where likely protoliths to high-grade residual granulites can be measured and more realistic estimates of the partial melting history of rocks can be discerned.

Using the mid amphibolite samples as likely protolith compositions for the higher grade samples, melt mode contours in Figure 6a, b show the maximum potential melt fertility of the metabasic rocks as a function of *P–T* conditions. The mode contours show that 30–35 mol.% (approximation of vol.%) melt could be produced at the highest grade conditions of 900–950°C under closed system melting.

The relationship between melt production and modal changes in the minerals can be illustrated in modebox plots. The plots in Figure 8a and 8b show the evolution of mineral assemblages, modes and melt abundance as a function of temperature along the metamorphic field gradient from 650°C at 5 kbar to 1000°C at 9.9 kbar. Assuming the mid amphibolite facies metabasic rocks represent approximate protoliths for the granulite facies (Kunz et al., 2014) this allows us to study the prograde history. In the mode box plot of Figure 8a hornblende, plagioclase and quartz represent the modally dominant phases until about 900°C when hornblende runs out. Figure 8b shows that also in sample IZ 014b hornblende, plagioclase and quartz modally dominate the mineral assemblage until 850°C, however biotite abundance is higher in this sample, in agreement with the observations in thin section. The breakdown of biotite at close to 850°C causes an increase in melt abundance. From thereon hornblende abundance decreases steadily but is not completely consumed until above 1000°C.

Figure 8c and 8d show the compositional evolution of melt produced by the same metabasic samples with increasing temperature along the metamorphic field gradient in the ternary anorthite (An), albite (Ab) and orthoclase (Or) compositional space using CIPW norms. The first melts produced in both samples modelled have a granitic composition which evolves with increasing *P–T* away from the Ab apex towards the Or–An join of the triangle. This compositional trend is largely driven by the breakdown of biotite and the release of K_2O into the melt and persists until biotite is completely consumed at ≈820°C in IZ 006 and ≈850°C in IZ 014b. At *P–T* conditions beyond the stability of biotite, the melt compositions trend away from the Or apex into the granodiorite and/or tonalite field as the breakdown of hornblende begins to dominate melt production. From the mode box diagrams and the melt composition plots, it can be seen that *P–T* range over which melt production is highest coincides with the melt compositional transition from granite to granodiorite.

5 DISCUSSION & CONCLUSIONS

The continuous crustal section in the Ivrea Zone exposing intercalated metapelitic and metabasic rocks provides an ideal opportunity to study how comparable *P*–*T* estimates derived from THERMOCALC are for different bulk rock types. Our study shows that it is possible to use metabasic rocks to infer *P*–*T* conditions, melting and melt loss for high-temperature metamorphic terranes that are consistent with those derived from metapelitic rocks. However, this does not imply that the models are perfect, they will all have associated errors and some mismatches between the models and rocks have been noted in other studies (e.g. Forshaw, Waters, Pattison, Palin, & Gopon, 2018).

5.1 Comparison of *P*–*T* estimates

Metabasic rocks from Val Strona di Omegna give a *P*–*T* range from 3–9 kbar and ~680–800°C at mid amphibolite facies conditions to 7.2–8.5 kbar at 830–860°C in the upper amphibolite facies and 7.2–9.8 kbar and 850–990°C for granulite facies samples (Figure 7a). These *P*–*T* conditions are in good agreement with previous estimates from forward modelling (3.5–11 kbar at 650 to <900°C; Redler et al., 2012, 2013) and Zr-in-rutile thermometry (910–930°C; Ewing et al., 2013; Luvizotto & Zack, 2009).

The assemblage fields in the mid amphibolite facies typically show a large range in *P*–*T* conditions (Green et al., 2016) and therefore do not provide well defined *P*–*T* estimates. Nevertheless the peak mineral assemblage fields for mid amphibolite facies metabasic samples IZ 006 and IZ 014b overlap and correlate well with those from metapelitic samples IZ 010 and IZ 061(Figures 7b and 9).

The *P*–*T* conditions inferred for the upper amphibolite facies samples IZ 035 and IV 051 do not show overlap with those from the nearest metapelite sample IV 020 (Figure 7b), with the assemblage field from the metabasic rocks lying at higher pressure and temperatures. However, within uncertainty (± 50–100°C and 1–2 kbar; Green et al., 2016) the *P*–*T* estimates derived from both rock types are in reasonable agreement (Figure 9). The lack of overlap could be due to (i) the failure to recognise a mineral present in thin section when determining the mineral assemblage or the absence of a phase in the thin section that is present in the larger sample used to derive the bulk rock. (ii) Changes in stability of mineral phases due to uncertainties in LOI determination or minor components (e.g. MnO, CO_2, F, …) not present in the NCKFMASHTO system. Or, (iii) issues with the thermodynamic data used in the calculations. Palin et al. (2016) showed that slight changes in

bulk rock composition, especially H_2O can affect the position of the solidus as well as other phases. For both samples (IZ 035 and IV 051), we needed to increase the H_2O content, from 1.44 mol.% to 3.3 mol.% and 1.27 mol.% to 3.2 mol.% in order to calculate a phase diagram which had the peak mineral assemblage observed in the samples. The adjusted H_2O content is similar to that of the mid amphibolite facies samples (see Table 2) and therefore a realistic H_2O content prior dehydration or melt loss. Nevertheless, there is some added uncertainty in the lower *T* limit of the upper amphibolite facies samples as the assemblage fields are defined by the solidus, which is highly dependent on water content of the rock (Palin et al., 2016). If these samples formed at slightly lower *P*–*T*, consistent with the nearby metapelite sample, the phase diagrams predict an identical assemblage but with the additional presence of biotite, which was not observed as a stable phase in the sample. However, this difference may reflect small inaccuracies in the *a*–*x* relationships used.

The granulite facies metabasic samples IZ 161 and IZ 100 overlap with the metapelitic sample IZ 070 (Figures 7b and 9). The fields in the granulite facies show a large range in temperature over a narrow range of pressure. At these conditions the assemblage field is limited towards higher temperatures by the hornblende-out reaction. To refine the peak *T* conditions we use the literature results derived from Zr-in-rutile thermometry along the metamorphic field gradient. The highest grade samples determined by Zr-in-rutile thermometry gives a maximum peak *T* of 930°C for Val Strona di Omegna (Ewing et al., 2013; Luvizotto & Zack, 2009). As our highest grade sample is slightly higher grade than those used for the Zr-in-rutile thermometry, we limit our peak *P*–*T* conditions to 940°C at 9 kbar along the metamorphic field gradient (Figure 7b).

5.2 Metamorphic field gradient

Based on the combination of constraints from both rock types we define a refined metamorphic field gradient (Figure 7b) for Val Strona di Omegna. Using the combined *P*–*T* estimates for the samples in this study results in a metamorphic field gradient from ~5 kbar at 650°C up to 940°C at 9 kbar. Similar to previous studies (e.g., Henk et al., 1997; Redler et al., 2012; Siegesmund et al., 2008) we have found no evidence for discontinuities in our modelled field gradient despite the presence of a high-temperature shear zone close to the amphibolite to granulite facies transition (Rosarolo shear zone). Nevertheless we cannot exclude the possibility of minor displacement undetectable within the uncertainties of our modelling.

In contrast the metamorphic field gradient in Val Strona di Omegna from Redler et al. (2012), based on phase equilibrium modelling of metapelitic rocks, showed a relative steep gradient from ~3.5–6.5 kbar at 650°C up to ~10–12 kbar above 900°C The updated version of the metamorphic field gradient based on both metabasic and metapelitic rocks calculated with the new thermodynamic dataset ds6 (Holland & Powell, 2011) is shallower. The consistency between the results derived from the metabasic rocks and those from the metapelitic rocks along the profile is shown in Figure 9. The lower pressures at higher temperatures of the metamorphic field gradient in this study are in better agreement with the inferred geological setting of crustal thinning and a higher heat flow due to astenospheric upwelling during the late Palaeozoic (Handy et al., 1999).

5.3 Melting & melt loss in metabasic rocks

The calculated modal abundance of melt (Figure 8a) show that sufficiently hydrated metabasic rocks in Val Strona di Omegna could produce up to 30 vol.% melt at the *P–T* conditions of the highest grade sample IZ 100. Field evidence based estimates for melt volume from Kunz et al. (2014) inferred 10–20 vol.% at the highest grades. This difference can be explained by melt loss or chemical variation (e.g. different degrees of hydration) in the protolith of amphibolite and granulite facies samples. Granulite facies metabasic rocks in this study have mostly anhydrous mineral assemblage and limited retrogression, therefore have undergone some melt loss (Palin et al., 2016; White & Powell, 2002). We present a simple closed system model for the modal abundance of mineral phases along the metamorphic field gradient together with the evolution of melt composition. The simple model approach used in this study does not take progressive prograde melt loss into account. Other studies using episodic melt loss models showed that due to the continuous melt loss the melt production at high grade is lower due to a reduced fertility after each melt loss event (Palin et al., 2016; Stuck & Diener, 2018; White & Powell, 2002; Yakymchuk & Brown, 2014).

The mode box plots (Figure 8a) show that only small amounts of melt would have been produced until the onset of biotite breakdown. Above this, the melt volume increases sharply with increasing *P–T*. This is in agreement with the observations from the field and thin section, where microscopic or macroscopic evidence for partial melting occurs in mostly biotite absent assemblages. Only the highest grade sample IZ 100 appears to have run out of hornblende during melting. The melt composition, modelled using THERMOCALC, evolves from granitic to granodioritic and finally tonalitic. This trend in melt composition is in good agreement with the observed composition of leucosomes in thin sections going up grade.

Figure 10 shows the bulk rock composition of the average upper amphibolite facies and average granulite facies metabasic rocks normalised to the average mid amphibolite facies metabasic rock composition adapted from Kunz et al. (2014). Additional to the relative depletion (Na, K, and possibly Si, Al) of upper amphibolite and granulite facies samples due to progressive metamorphism and melt loss. We show that the predicted granulite facies rock compositions modelled from mid amphibolite facies samples (extracted with the rbi function in THERMOCALC) are consistent with the trends seen in natural average granulite facies compositions. The bulk rock composition of the melt-depleted residuum extracted at peak conditions from the mid amphibolite facies bulk rock composition shows lower K_2O content than those of the average granulite facies. This could be due to the fact that the bulk rock composition is extracted at the highest grade conditions experienced in the region whereas some samples used to calculate the average granulite facies bulk rock composition likely experienced peak conditions below this regional maximum. Furthermore as discussed in more detail by Kunz et al. (2014) it is possible that there has been some contamination from K_2O-rich melt or fluids derived from the surrounding metapelitic rocks into metabasic rocks. However the K_2O concentration of IZ 100 (highest grade samples) is very similar to that derived from THERMOCALC modelling of melt-depleted residua.

The possibility of using metabasic and metapelitic rocks interchangeably or combined to derive *P–T* conditions for metamorphic terranes is of great advantage. With our study we have shown that the new *a–x* models (Green et al., 2016) produce results consistent with those derived from the metapelite models of White et al. (2014), at least for the *P–T* conditions and rock compositions preserved in the Ivrea zone.

ACKNOWLEDGEMENTS

We thank C. Redler for discussions and assistance in the field. We are grateful to M.C. De Paoli and an anonymous reviewer for their constructive reviews and to D. Robinson for editorial handling. The authors declare they have no conflicts of interest.

REFERENCES

Barboza, S., & Bergantz, G. (2000). Metamorphism and Anatexis in the Mafic Complex Contact Aureole, Ivrea Zone, Northern Italy. *Journal Petrology, 41*, 1307–1327.

Barboza, S., Bergantz, G., & Brown, M. (1999). Regional granulite facies metamorphism in the Ivrea zone Is the Mafic Complex the smoking gun or a red herring. *Geology, 27*, 447–450.

Bea, F., & Montero, P. (1999). Behavior of accessory phases and redistribution of Zr, REE, Y, Th, and U during metamorphism and partial melting of metapelites in the lower crust: an example from the Kinzigite Formation of Ivrea-Verbano, NW Italy. *Geochimica et Cosmochimica Acta, 63*, 1133–1153.

Bertolani, M. (1968). La petrografia della Valle Strona (Alpi Occidentali Italiane). *Schweizerische Mineralogische und Petrographische Mitteilungen, 48*, 695–733.

Bigi G., & Carrozzo M. T. (1990). Structural model of Italy and gravity map. *Consiglio Nazionale delle Ricerche (Italia), 114,* 3.

Binns, R. A. (1964). Zones of progressive regional metamorphism in the Willyama complex, Broken Hill district, New South Wales. *Journal of the Geological Society of Australia, 11,* 283–330.

Boriani, A., Burlini, L., & Sacchi, R. (1990). The Cossato-Mergozzo-Brissago Line and the Pogallo Line (Southern Alps, Northern Italy) and their relationships with the late-Hercynian magmatic and metamorphic events. *Tectonophysics, 182*, 91–102.

Brown, M., & Rushmer, T. (2006). *Evolution and differentiation of the continental crust*. Cambridge University Press.

Chapman, T., Clarke, G. L., Piazolo, S., & Daczko, N. R. (2017). Evaluating the importance of metamorphism in the foundering of continental crust. *Scientific Reports, 7*, 13039.

Dale, J., Powell, R., White, R. W., Elmer, F. L., & Holland, T. J. (2005). A thermodynamic model for Ca-Na clinoamphiboles in Na_2O-CaO-FeO-MgO-Al_2O_3-SiO_2-H_2O-O for petrological calculations. *Journal of Metamorphic Geology, 23*, 771–791.

Diener, J. F., & Powell, R. (2012). Revised activity-composition models for clinopyroxene and amphibole. *Journal of Metamorphic Geology, 30*, 131–142.

Diener, J. F., Powell, R., White, R. W., & Holland, T. J. (2007). A new thermodynamic model for clino- and orthoamphiboles in the system Na_2O-CaO-FeO-MgO-Al_2O_3-SiO_2-H_2O-O. *Journal of Metamorphic Geology*, *25*, 631–656.

Ewing, T. A., Hermann, J., & Rubatto, D. (2013). The robustness of the Zr-in-rutile and Ti-in-zircon thermometers during high-temperature metamorphism (Ivrea-Verbano Zone, northern Italy). *Contributions to Mineralogy and Petrology*, *165*, 757–779.

Feisel, Y., White, R. W., Palin, R. M., & Johnson, T. E. (2018). New constraints on granulite facies metamorphism and melt production in the Lewisian Complex, northwest Scotland. *Journal of Metamorphic Geology*, *36*, 799–819.

Forshaw, J.B., Waters, D. J., Pattison, D. R. M., Palin, R. M., & Gopon, P. A. (2018). Comparison of observed and thermodynamically predicted phase equilibria and mineral compositions in mafic granulites. *Journal of Metamorphic Geology*, https://doi.org/10.1111/jmg.12454.

Gansser, A. (1968). The insubric line, a major geotectonic problem. *Schweizerische Mineralogische und Petrographische Mitteilungen*, *48*, 123–143.

Green, E. C., Holland, T. J., & Powell, R. (2007). An order-disorder model for omphacitic pyroxenes in the system jadeite-diopside-hedenbergite-acmite, with applications to eclogitic rocks. *American Mineralogist*, *92*, 1181–1189.

Green, E. C., White, R. W., Diener, J. F., Powell, R., Holland, T. J., & Palin, R. M. (2016). Activity–composition relations for the calculation of partial melting equilibria in metabasic rocks. *Journal of Metamorphic Geology*, *34*, 845–869.

Greenfield, J. E., Clarke, G. L., & White, R. W. (1998). A sequence of partial melting reactions at Mt Stafford, central Australia. *Journal of Metamorphic Geology*, *16*, 363–378.

Handy, M. R. (1987). The structure, age and kinematics of the Pogallo Fault Zone; Southern Alps, northwestern Italy. *Eclogae Geologicae Helvetiae*, *80*, 593–632.

Harley, S. L. (2016). A matter of time: the importance of the duration of UHT metamorphism. *Journal of Mineralogical and Petrological Sciences*, *111*, 50–72.

Hartel, T. H. D., & Pattison, D. R. M. (1996). Genesis of the Kapuskasing (Ontario) migmatitic mafic granulites by dehydration melting of amphibolite: the importance of quartz to reaction progress. *Journal of Metamorphic Geology 14*, 591–611.

Handy, M. R., Franz, L., Heller, F., Janott, B., & Zurbriggen, R. (1999). Multistage accretion and exhumation of the continental crust (Ivrea crustal section, Italy and Switzerland). *Tectonics, 18*, 1154–1177.

Henk, A., Franz, L., Teufel, S., & Oncken, O. (1997). Magmatic Underplating, Extension, and Crustal Reequilibration: Insights from a Cross-Section through the Ivrea Zone and Strona-Ceneri Zone, Northern Italy. *The Journal of Geology, 105*, 367–377.

Holland, T. J., & Powell, R. (2003). Activity-composition relations for phases in petrological calculations: an asymmetric multicomponent formulation. *Contributions to Mineralogy and Petrology, 145*, 492–501.

Holland, T. J., & Powell, R. (2011). An improved and extended internally consistent thermodynamic dataset for phases of petrological interest, involving a new equation of state for solids. *Journal of Metamorphic Geology, 29*, 333–383.

Johnson, T. E., & Brown, M. (2004). Quantitative Constraints on Metamorphism in the Variscides of Southern Brittany - a Complementary Pseudosection Approach. *Journal of Petrology, 45*, 1237–1259.

Johnson, T. E., & White, R. W. (2011). Phase equilibrium constraints on conditions of granulite-facies metamorphism at Scourie, NW Scotland. *Journal of the Geological Society, 168*, 147–158.

Johnson, T. E., Fischer, S., White, R. W., Brown, M., & Rollinson, H. R. (2012). Archaean Intracrustal Differentiation from Partial Melting of Metagabbro - Field and Geochemical Evidence from the Central Region of the Lewisian Complex, NW Scotland. *Journal of Petrology, 53*, 2115–2138.

Johnson, T. E., Kirkland, C. L., Reddy, S. M., & Fischer, S. (2015). Grampian migmatites in the Buchan Block, NE Scotland. *Journal of Metamorphic Geology, 33*, 695–709.

Kelsey, D. E., & Hand, M. (2015). On ultrahigh temperature crustal metamorphism: phase equilibria, trace element thermometry, bulk composition, heat sources, timescales and tectonic settings. *Geoscience Frontiers, 6*, 311–356.

Korhonen, F. J., Saito, S., Brown, M., & Siddoway, C. S. (2010). Modeling multiple melt loss events in the evolution of an active continental margin. *Lithos, 116*, 230–248.

Kunz, B. E., Johnson, T. E., White, R. W., & Redler, C. (2014). Partial melting of metabasic rocks in Val Strona di Omegna, Ivrea Zone, northern Italy. *Lithos, 190–191*, 1–12.

Kunz, B. E., Regis, D., & Engi, M. (2018). Zircon ages in granulite facies rocks: decoupling from geochemistry above 850 °C? *Contributions to Mineralogy and Petrology, 173*, 26.

Luvizotto, G. L., & Zack, T. (2009). Nb and Zr behavior in rutile during high-grade metamorphism and retrogression: An example from the Ivrea-Verbano Zone. *Chemical Geology, 261*, 303–317.

Mulch, A., Cosca, M., & Handy, M. (2002). In-situ UV-laser $^{40}Ar/^{39}Ar$ geochronology of a micaceous mylonite : an example of defect-enhanced argon loss. *Contributions to Mineralogy and Petrology, 142*, 738–752.

Mulch, A., Rosenau, M., & Doerr, W. (2002). The age and structure of dikes along the tectonic contact of the Ivrea-Verbano and Strona-Ceneri Zones (southern Alps, Northern Italy, Switzerland). *Schweizerische Mineralogische und Petrographische Mitteilungen, 82*, 55–76.

Palin, R. M., White, R. W., Green, E. C., Diener, J. F., Powell, R., & Holland, T. J. (2016). High-grade metamorphism and partial melting of basic and intermediate rocks. *Journal of Metamorphic Geology, 34*, 871–892.

Palin, R. M., White, R. W., & Green, E. C. (2016). Partial melting of metabasic rocks and the generation of tonalitic-trondhjemitic-granodioritic (TTG) crust in the Archaean: constraints from phase equilibrium modelling. *Precambrian Research, 287*, 73–90.

Peressini, G., Quick, J. E., Sinigoi, S., Hofmann, A. W., & Fanning, M. (2007). Duration of a Large Mafic Intrusion and Heat Transfer in the Lower Crust: a SHRIMP U-Pb Zircon Study in the Ivrea-Verbano Zone (Western Alps, Italy). *Journal Petrology, 48*, 1185–1218.

Powell, R., & Holland, T. J. (1988). An internally consistent dataset with uncertainties and correlations: 3. Applications to geobarometry, worked examples and a computer program. *Journal of Metamorphic Geology, 6*, 173–204.

Quick, J. E., Sinigoi, S., Negrini, L., Demarchi, G., & Mayer, A. (1992). Synmagmatic deformation in the underplated igneous complex of the Ivrea-Verbano zone. *Geology, 20*, 613–616.

Quick, J. E., Sinigoi, S., Snoke, A. W., Kalakay, T. J., Mayer, A., & Peressini, G. (2003). Geologic Map of the Southern Ivrea-Verbano Zone, Northwestern Italy. *USGS, I–2776*, 1–22.

Redler, C., Johnson, T. E., White, R. W., & Kunz, B. E. (2012). Phase equilibrium constraints on a deep crustal metamorphic field gradient: metapelitic rocks from the Ivrea Zone (NW Italy). *Journal of Metamorphic Geology*, *30*, 235–254.

Redler, C., White, R. W., & Johnson, T. E. (2013). Migmatites in the Ivrea Zone (NW Italy): Constraints on partial melting and melt loss in metasedimentary rocks from Val Strona di Omegna. *Lithos*, *175–176*, 40–53.

Reinsch, D. (1973a). Die Metabasite des Valle Strona (Ivrea Zone). *Neues Jahrbuch Mineralogische Abhandlungen*, *118*, 190–210.

Reinsch, D. (1973b). Die Metabasite des Valle Strona (Ivrea Zone) (2.Teil). *Neues Jahrbuch Mineralogische Abhandlungen*, *119*, 266–284.

Rudnick, R. L., & Fountain, D. M. (1995). Nature and composition of the continental crust: a lower crustal perspective. *Reviews of Geophysics*, *33*, 267–309.

Rushmer, T. (1991). Partial melting of two amphibolites: contrasting experimental results under fluid-absent conditions. *Contributions to Mineralogy and Petrology*, *107*, 41–59.

Rutter, E., Brodie, K., James, T., & Burlini, L. (2007). Large-scale folding in the upper part of the Ivrea-Verbano zone, NW Italy. *Journal of Structural Geology*, *29*, 1–17.

Sawyer, E.W. (1991). Disequilibrium melting and the rate of melt–residuum separation during migmatization of mafic rocks from the Grenville Front, Quebec. *Journal of Petrology*, *32*, 701–738.

Sawyer, E. W. (2008). *Atlas of Migmatites* (Vols. The Canadian Mineralogist, Special Publications 9). (E. W. Sawyer, Ed.) NRC Research Press, Ottawa, Ontario, Canada.

Schmid, R., & Wood, B. J. (1976). Phase relationships in granulitic metapelites from the Ivrea-Verbano zone (Northern Italy). *Contributions to Mineralogy and Petrology*, *54*, 255–279.

Schmid, S. M. (1993). *Pre-Mesozoic geology in the Alps*. In J. F. Raumer, & F. Neubauer (Eds.). Springer.

Schmid, S. M., Zingg, A., & Handy, M. (1987). The kinematics of movements along the Insubric Line and the emplacement of the Ivrea Zone. *Tectonophysics*, *135*, 47–66.

Siegesmund S., Layer P., Dunkl I., Vollbrecht A., Steenken A., Wemmer K., & Ahrendt, H. (2008). Exhumation and deformation history of the lower crustal section of the Valstrona di Omegna in the Ivrea Zone, southern Alps. *Geological Society, London, Special Publications, 298,* 45–68.

Sills, J. D., & Tarney, J. (1984). Petrogenesis and tectonic significance of amphibolites interlayered with metasedimentary gneisses in the Ivrea Zone, Southern Alps, northwest Italy. *Tectonophysics, 107*, 187–206.

Sinigoi, S., Antonini, P., Demarchi, G., Longinelli, A., Mazzucchelli, M., Negrini, L., & Rivalenti, G. (1991). Intractions of mantle and crustal magmas in the southern part of the Ivrea Zone (Italy). *Contributions to Mineralogy and Petrology, 108,* 385–395.

Sinigoi, S., Quick, J. E., Mayer, A., & Budahn, J. (1996). Influence of stretching and density contrasts on the chemical evolution of continental magmas: an example from the Ivrea-Verbano Zone. *Contributions to Mineralogy and Petrology, 123,* 238–250.

Sinigoi, S., Quick, J. E., Demarchi, G., & Klötzli, U. (2011). The role of crustal fertility in the generation of large silicic magmatic systems triggered by intrusion of mantle magma in the deep crust. *Contributions to Mineralogy and Petrology, 162*, 691–707.

Stuck, T. J., & Diener, J. F. (2018). Mineral equilibria constraints on open-system melting in metamafic compositions. *Journal of Metamorphic Geology, 36*, 255–281.

Vavra, G., Schmid, R., & Gebauer, D. (1999). Internal morphology, habit and U-Th-Pb microanalysis of amphibolite-to-granulite facies zircons: geochronology of the Ivrea Zone (Southern Alps). *Contributions to Mineralogy and Petrology, 134*, 380–404.

Waters, D. J. (1986). Metamorphic history of sapphirine-bearing and related magnesian gneisses from Namaqualand, South Africa. *Journal of Petrology, 27*, 541–565.

White, R. W., & Powell, R. (2002). Melt loss and the preservation of granulite facies mineral assemblages. *Journal of Metamorphic Geology, 20*, 621–632.

White, R. W., Powell, R., & Holland, T. J. (2001). Calculation of partial melting equilibria in the system Na_2O-CaO-K_2O-FeO-MgO-Al_2O_3-SiO_2-H_2O (NCKFMASH). *Journal of Metamorphic Geology, 19*, 139–153.

White, R. W., Powell, R., & Clarke, G. L. (2002). The interpretation of reaction textures in Fe-rich metapelitic granulites of the Musgrave Block, central Australia: constraints from mineral equilibria calculations in the system K_2O-FeO-MgO-Al_2O_3-SiO_2-H_2O-TiO_2-Fe_2O_3. *Journal of Metamorphic Geology, 20*, 41–55.

White, R. W., Powell, R., & Clarke, G. L. (2003). Prograde metamorphic assemblage evolution during partial melting of metasedimentary rocks at low pressures: migmatites from Mt Stafford, Central Australia. *Journal of Petrology, 44*, 1937–1960.

White, R. W., Powell, R., & Halpin, J. A. (2004). Spatially-focussed melt formation in aluminous metapelites from Broken Hill, Australia. *Journal of Metamorphic Geology, 22*, 825–845.

White, R. W., Pomroy, N. E., & Powell, R. (2005). An in situ metatexite-diatexite transition in upper amphibolite facies rocks from Broken Hill, Australia. *Journal of Metamorphic Geology, 23*, 579–602.

White, R. W., Powell, R., Holland, T. J., Johnson, T. E., & Green, E. C. (2014). New mineral activity-composition relations for thermodynamic calculations in metapelitic systems. *Journal of Metamorphic Geology, 32*, 261–286.

White, R. W., Palin, R. M., & Green, E. C. (2017). High-grade metamorphism and partial melting in Archean composite grey gneiss complexes. *Journal of Metamorphic Geology, 35*, 181–195.

Wyllie, P. J., & Wolf, M. B. (1993). Amphibolite dehydration-melting: sorting out the solidus. *Geological Society, London, Special Publications, 76*, 405–416.

Yakymchuk, C. (2017). Applying Phase Equilibria Modelling to Metamorphic and Geological Processes: Recent Developments and Future Potential. *Geoscience Canada, 44*, 27–45.

Yakymchuk, C., & Brown, M. (2014). Behaviour of zircon and monazite during crustal melting. *Journal of the Geological Society, 171*, 465–479.

Zingg, A. (1978). *Regionale Metamorphose in der Ivrea Zone (Nord-Italien)*. Ph.D. thesis, ETH Zürich, Switzerland.

Zingg, A. (1980). Regional Metamorphism in the Ivrea Zone (Southern Alps, N-Italy): Field and microscopic Investigations. *Schweizerische Mineralogische und Petrographische Mitteilungen, 60*, 153–179.

Zingg, A., Handy, M. R., Hunziker, J. C., & Schmid, S. M. (1990). Tectonometamorphic history of the Ivrea Zone and its relationship to the crustal evolution of the Southern Alps. *Tectonophysics, 182*, 169–192.

SUPPORTING INFORMATION

Additional Supporting Information may be found online in the supporting information tab for this article.

Figure S1: Map of Val Strona di Omegna as in Figure 2 with the addition of the geological map redrawn after Bertolani (1986)

Figure S2: Fully labelled *P*–*T* pseudosection presented in Figure 6

Figure S3: *T*–*x* diagram for H_2O content of upper amphibolite facies samples IZ 035 and IV 051 at 7 kbar

Figure S4: Comparison of peak assemblage fields of the metapelitic rocks from Redler et al. (2012) calculated with ds55 and those of this study calculated with ds66

Figure Captions

Figure 1 Geological overview map of the Ivrea Zone (N-Italy). The map is redrawn after Bigi and Carrozzo (1990), Rutter et al. (2007) and Zingg (1980)

Figure 2 Schematic map of Val Strona di Omegna with mineral isograds (taken from Kunz et al., 2014; Redler et al., 2012) and sample localities of metabasic rocks (stars) from this study and metapelitic samples (circles) from Redler et al. (2012). For a more detailed version of this map please refer to Figure S1

Figure 3 Field photographs of representative metabasic rocks from the Kinzigite Formation, Val Strona di Omegna. **(a)** Fine grained metabasic rock with folded quartz (q) vein in the mid amphibolite facies. **(b)** Layered metabasic rock from the upper amphibolite facies with segregation of melanocratic (M) and leucocratic (L) material. **(c)** First mesoscopic evidence for partial melting in metabasic rocks *c.* 1 km south of the amphibolite to granulite facies transition zone. Patches of segregated leucosome (L) made of plagioclase and quartz with coarse-grained peritectic clinopyroxene (aug) crystals surrounded by melanosome (M) consisting of mostly hornblende and plagioclase. **(d)** Metabasic migmatite with leucocratic (L) material forming pockets which are

connected via leucocratic networks. At the interface of the leucosome (L) to the melanosome (M) it occasionally mafic selvage of hornblende (hb) can be observed **(e)** Metatexitic metabasic rock from the lower granulite facies. Leucosome (L) enriched in clinopyroxene pools in the low pressure sites of the boudinaged melanosome (M). On the right side of the image a cm-sized leucocratic vein (L) is visible. **(f)** Metabasic migmatite from the granulite facies were smaller leucosome veins (L) with abundant coarse-grained peritectic clinopxroxene (cpx) form networks feeding into larger leucosome veins

Figure 4 Photomicrographs of metabasic rocks from Val Strona di Omegna (scale bar 1 mm). **(a)** Typical mid amphibolite facies sample (IZ 014b) with green hornblende and brown biotite making up the majority of the rock. Hornblende and biotite often show intergrowth. **(b)** Upper amphibolite facies sample (IZ 035) with clinopyroxene porphyroblasts, green hornblende, plagioclase, quartz and sphene. **(c)** Metabasic rock close to the amphibolite-granulite facies transition with a mineral assemblage of clinopyroxene, hornblende, plagioclase, quartz and ilmenite. Hornblende occurs in the matrix as well as replacing clinopyroxene. **(d)** Metabasic rock showing the typical granulite facies mineral assemblage clinopyroxene, orthopyroxene, hornblende, plagioclase, and ilmenite. Biotite is only present sporadically. **(e)** Thin section scan of the first field based evidence for partial melting. The left side of the image shows the metabasic rock with a slightly restitic composition dominated by hornblende. Towards the left the leucosome is dominated by plagioclase and quartz with large peritectic clinopyroxene crystals**.** In many cases clinopyroxene crystals show an overgrowth of hornblende. **(f)** Metabasic rock from Campello Monti (highest grade sample) with garnet, clino- and orthopyroxene porphyroblasts in a plagioclase matrix. Brown hornblende only occurs as inclusions in garnet or pyroxene or small relics within the matrix. Without clear overgrowth relationships it is usually not possible to distinguish between prograde and retrograde growth of the relic hornblende in the matrix

Figure 5 Field sketches from metabasic rocks from Val Strona di Omegna. **(a)** First evidence for leucocratic segregation visible in the field, in a metabasic rocks ~500m south of the village Rosarolo at sample locality IV 051. In several places small isolated pockets of leucocratic material form, which then aggregate into several cm big leucosome. The leucosome consists of mostly feldspar and quartz with coarse-grained peritectic clinopxroxene, occasionally overgrown or replaced by hornblende. **(b)** Metabasic migmatite from the lower

granulite facies were leucocratic veins with abundant coarse-grained peritectic clinopxroxene form a extended network around schollen of mostly melanosome or rarely paleosome

Figure 6 *P–T* pseudosection for six metabasic rocks from Val Strona di Omegna from mid amphibolite **(a, b)**, upper amphibolite facies **(c, d)** and granulite facies **(e, f)**. Inferred peak assemblage fields are highlighted in each pseudosection with mineral assemblage in bold. The bold black line marks the solidus and the dashed black line marks the hornblende out. The two mid amphibolite facies samples (a, b) are contoured for the modal abundance melt (dashed white lines). A fully labelled version of the *P–T* pseudosection can be found in the Figure S2

Figure 7 Metamorphic field gradient for Val Strona di Omegna. **(a)** Metamorphic field gradient based on peak mineral assemblage fields from metabasic rocks. Peak assemblage fields are coloured according to their metamorphic grade. **(b)** Metamorphic field gradient based on the combination of metapelitic and metabasic rocks (outlined bold) from the Kinzigite Formation in Val Strona di Omegna. For comparison the metamorphic field gradient from Redler et al. (2012) is shown as dashed lines. A direct comparison of the peak metamorphic assemblage field from Redler et al. (2012) with those of the present study can be found in Figure S4

Figure 8 Mode box diagrams for sample **(a)** IZ 006 and **(b)** IZ 014b. **(c)** and **(d)** Ternary diagrams (Ab, Or, An) showing melt composition evolution along the metamorphic field gradient

Figure 9 *P–T* estimates for the individual samples along the crustal section, with increasing distance from the CMB line the metamorphic grade increases. Both rock types (metabasic and metapelitic) give, within uncertainties (± 50–100°C and 1–2 kbar; Green et al., 2016), the same *P–T* conditions at approx. the same depth and metamorphic grade

Figure 10 Diagram showing the average major element composition of upper amphibolite facies (triangles) and granulite facies (circles) samples normalised to the average mid amphibolite facies composition taken from Kunz et al. (2014). Additionally plotted are the composition of sample IZ 006 and IZ 014b as well as the calculated residuum bulk rock composition (THERMOCALC rbi) of sample IZ 006 and IZ 014b at 940°C and 9 kbar normalised to the average mid amphibolite facies

Table Captions

Table 1 List of samples, locality, mineral assemblage and calculated *P*–*T* conditions of metabasic rocks from Val Strona di Omegna

Table 2 Bulk rock composition (mol.%) for metabasic rocks from Val Strona di Omegna used in peusdosection calculations. H_2O values for IZ 035 and IV 051 used for pseudosection calculation have been adjusted (see text details) original H_2O values determined by LOI are given in brackets

Table 1

Sample	Lithology	Locality	Coordinates		Mineral assemblage								*P–T* conditions	
			E	N	G	Opx	Aug	Hb	Pl	Q	Ilm	Bi	**P** (kbar)	**T** (°C)
Mid amphibolite facies														
IZ 006	Amphibolite	Germagno	452603	5082335				x	x	x	x	x	3–7.6	680–770
IZ 014b	Amphibolite	Loreglia	451414	5083567				x	x	x	x	x	3–9	700–800
Upper amphibolite facies														
IZ 035	Cpx-amphibolite	Marmo	446520	5084830			x	x	x	x	x	x	7.2–8.5	830–850
IV 051	Metabasic migmatite	Rosarolo	445186	5086123			x	x	x	x	x	x	6.7–8.5	840–860
Granulite facies														
IZ 161	Metabasic migmatite	Piana di Forno	443516	5086975	x	x	x	x	x	x	x	x	7.2–9.5	850–1050
IZ 100	Metabasic migmatite	Campello Monti	440934	5087103	x	x	x	(x)	x	(x)	x	(x)	7.3–9.8	940–990

Table 2

	Bulk rock composition (mol.%)									
Sample	**H_2O**	**SiO_2**	**Al_2O_3**	**CaO**	**MgO**	**FeO**	**K_2O**	**Na_2O**	**TiO_2**	**O**
Mid amphibolite facies										
IZ 006	3.08	58.50	11.55	9.55	5.85	7.26	0.48	3.46	0.69	0.80
IZ 014b	4.78	54.90	11.88	9.06	8.76	6.28	0.88	2.74	0.99	0.46
Upper amphibolite facies										
IZ 035	3.3 (1.44)	51.00	8.50	13.44	11.79	10.71	0.34	2.08	1.25	0.78
IV 051	3.2 (1.27)	50.15	8.96	11.41	11.21	13.85	0.36	2.45	2.35	2.51
Granulite facies										
IZ 161	1.85	50.07	11.48	12.90	8.42	10.99	0.47	2.41	1.88	1.03
IZ 100	0.26	52.39	13.32	11.75	7.75	10.25	0.23	2.91	1.30	0.78
Modelled residuum @ 940°C & 9 kbar										
IZ 006	0.44	55.63	12.33	11.22	6.99	7.91	0.16	3.41	0.89	1.03
IZ 014b	1.81	50.97	12.73	10.79	11.36	7.35	0.26	2.76	1.35	0.63

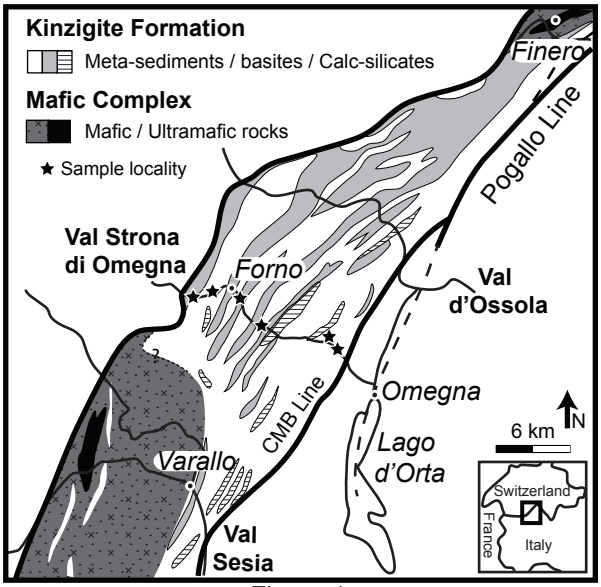

Figure 1

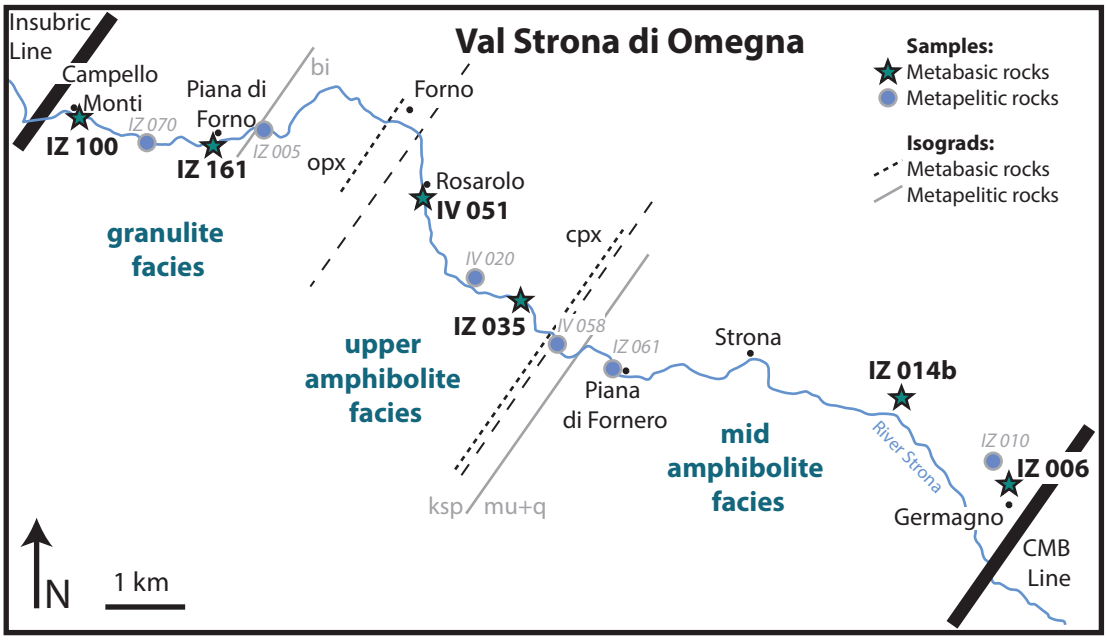

Figure 2

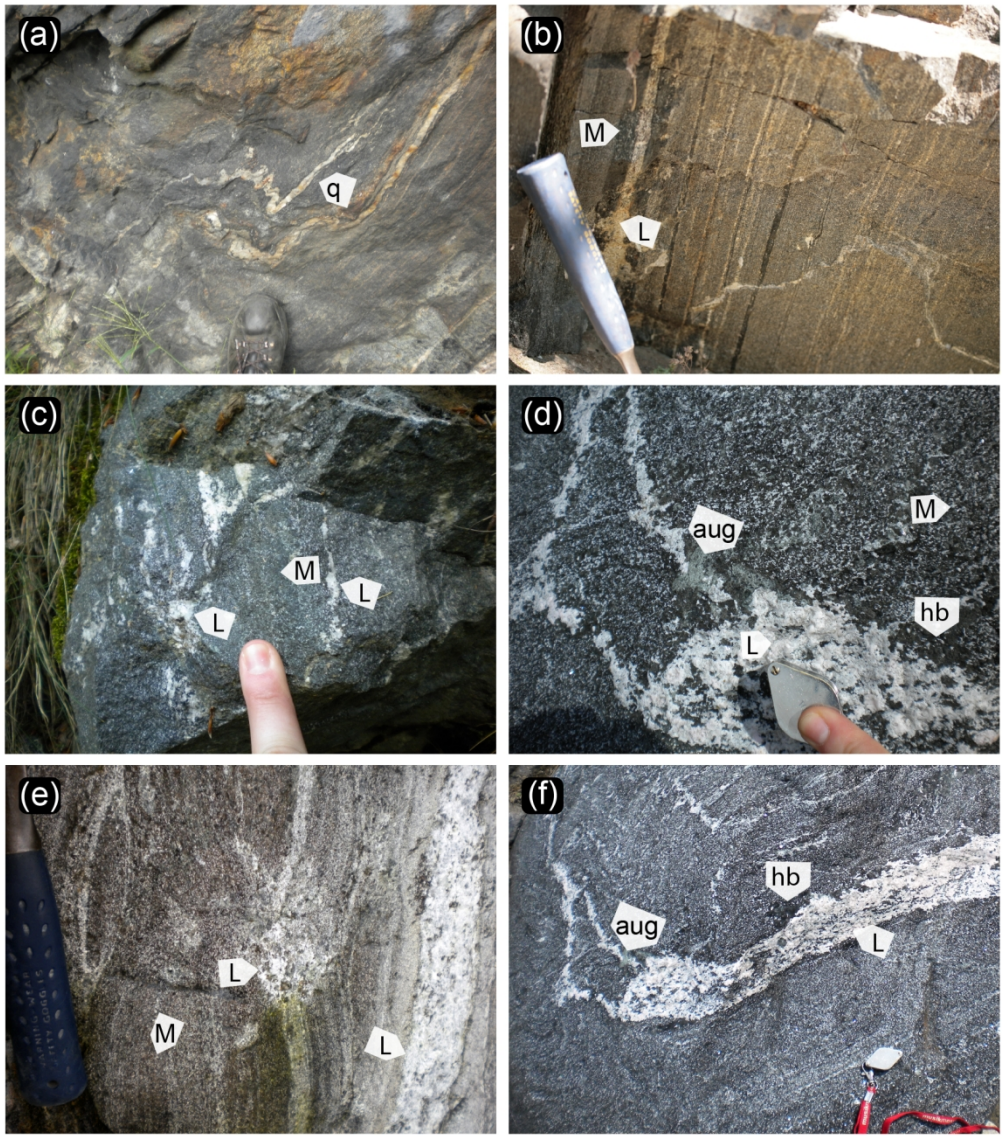

Figure 3

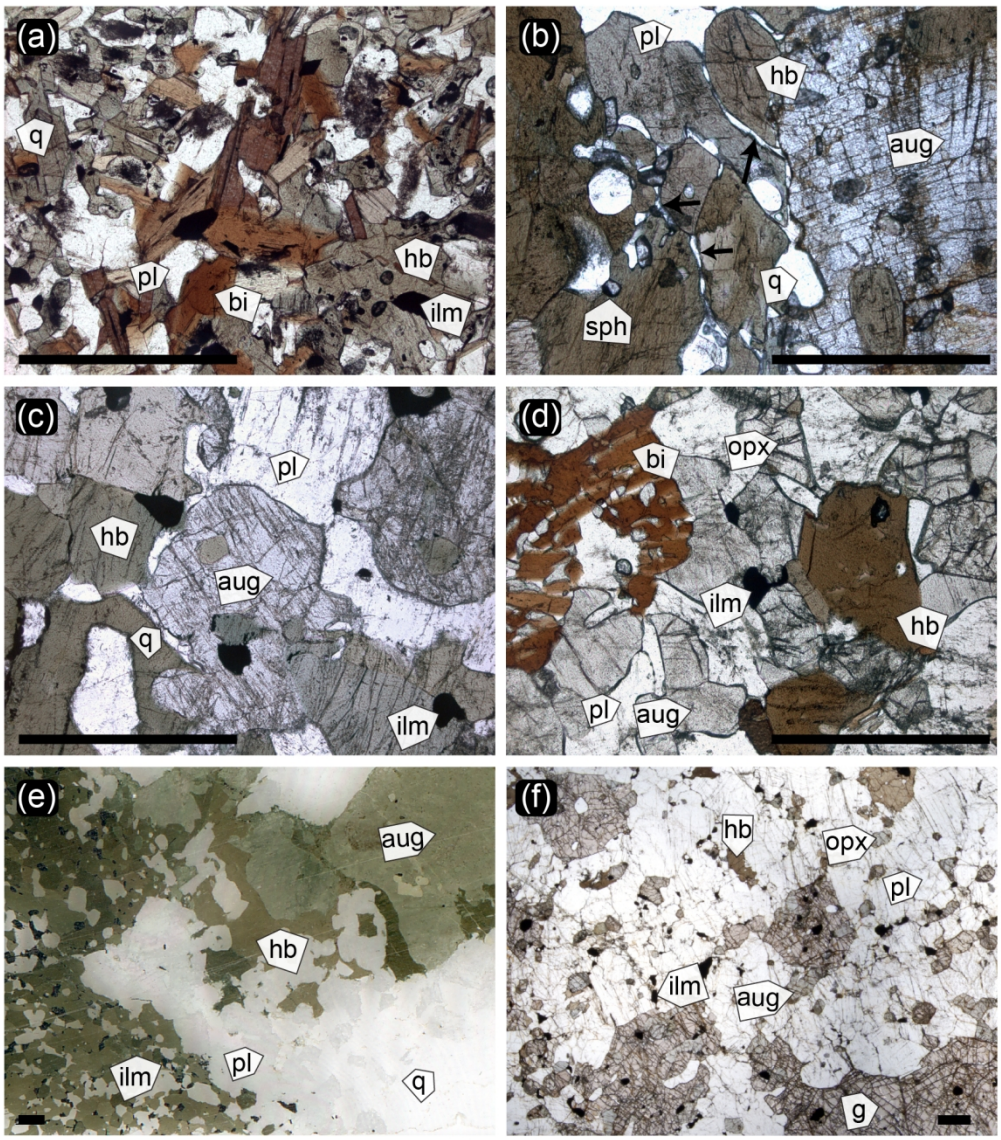

Figure 4

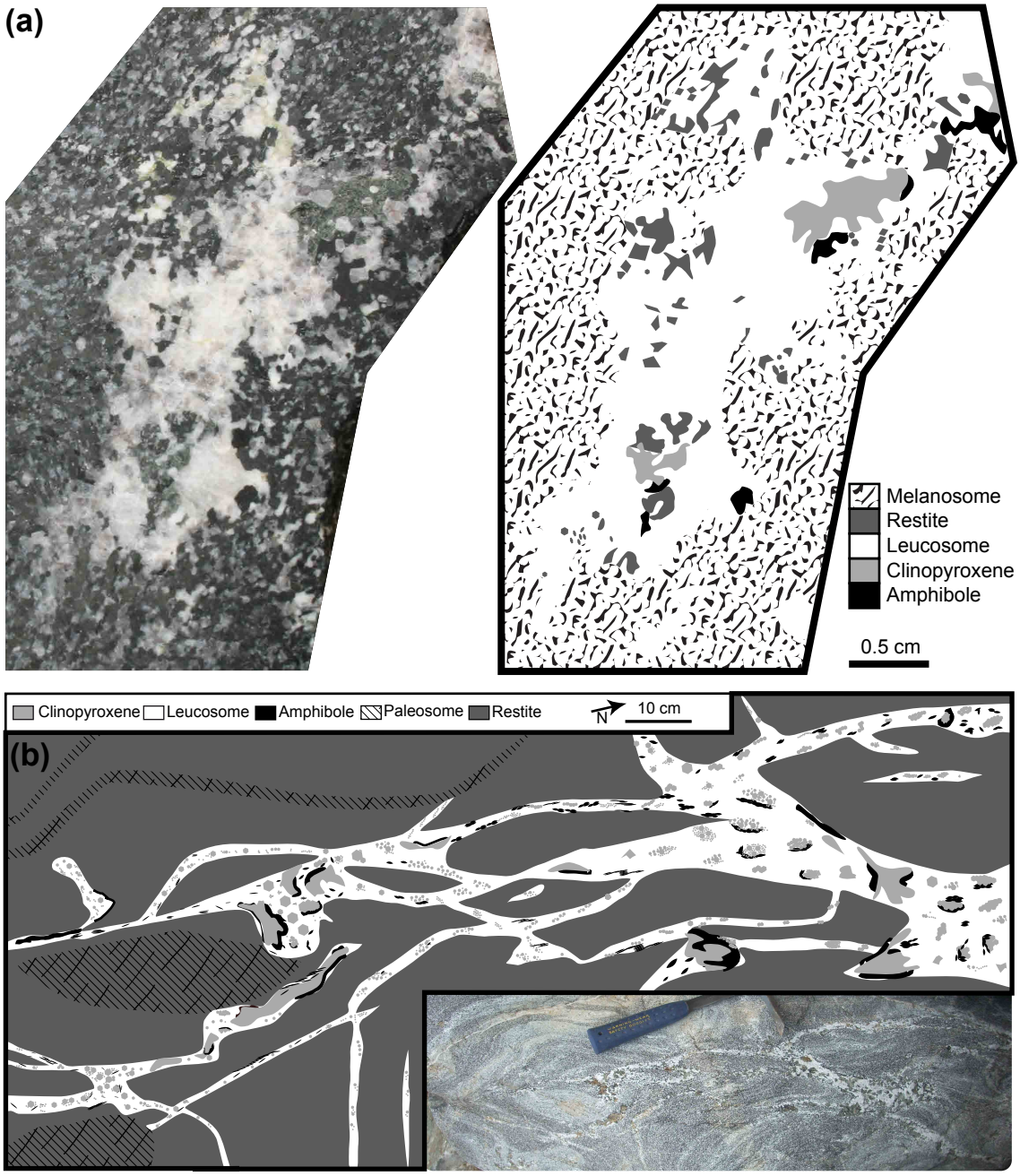

Figure 5

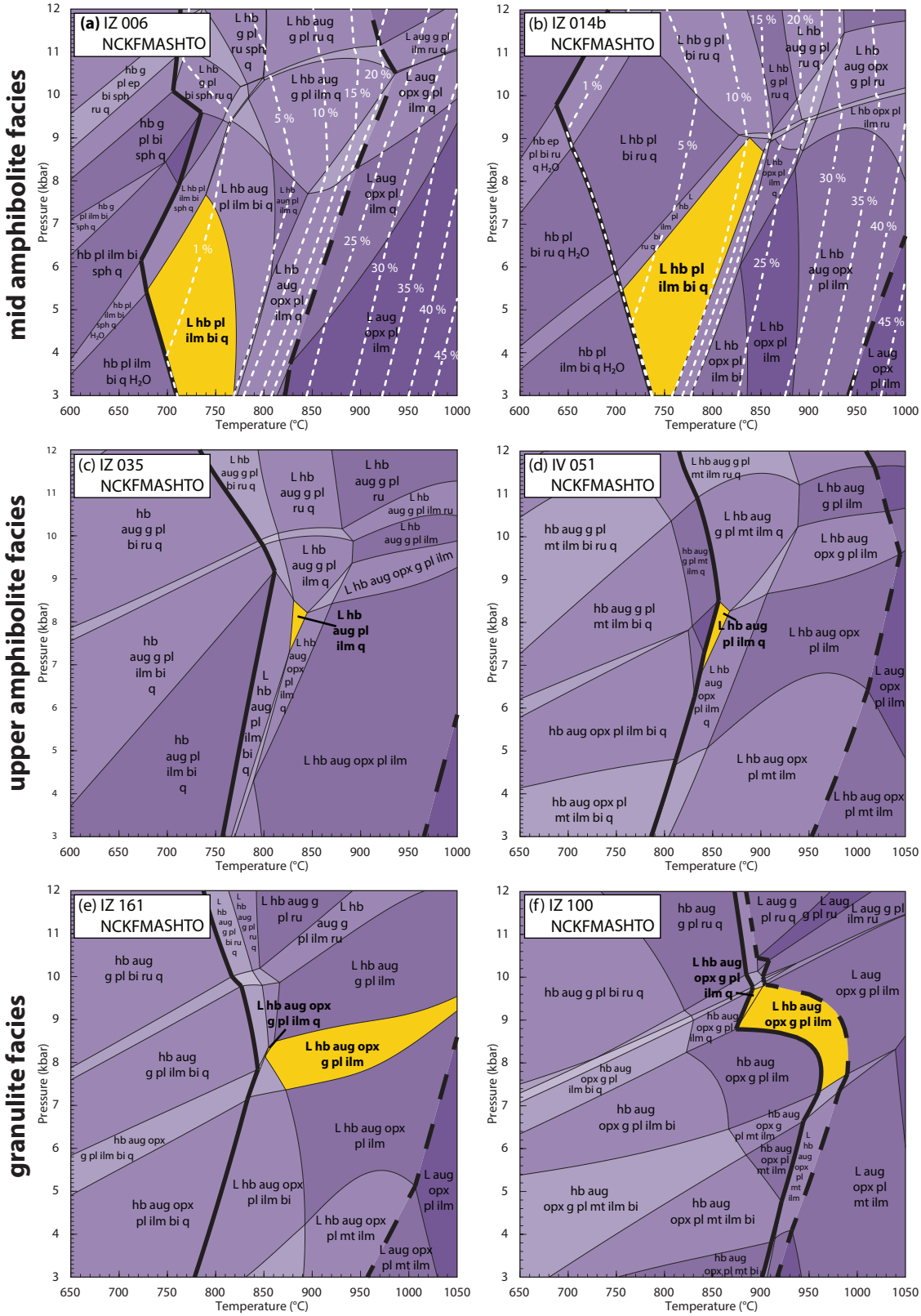

Figure 6

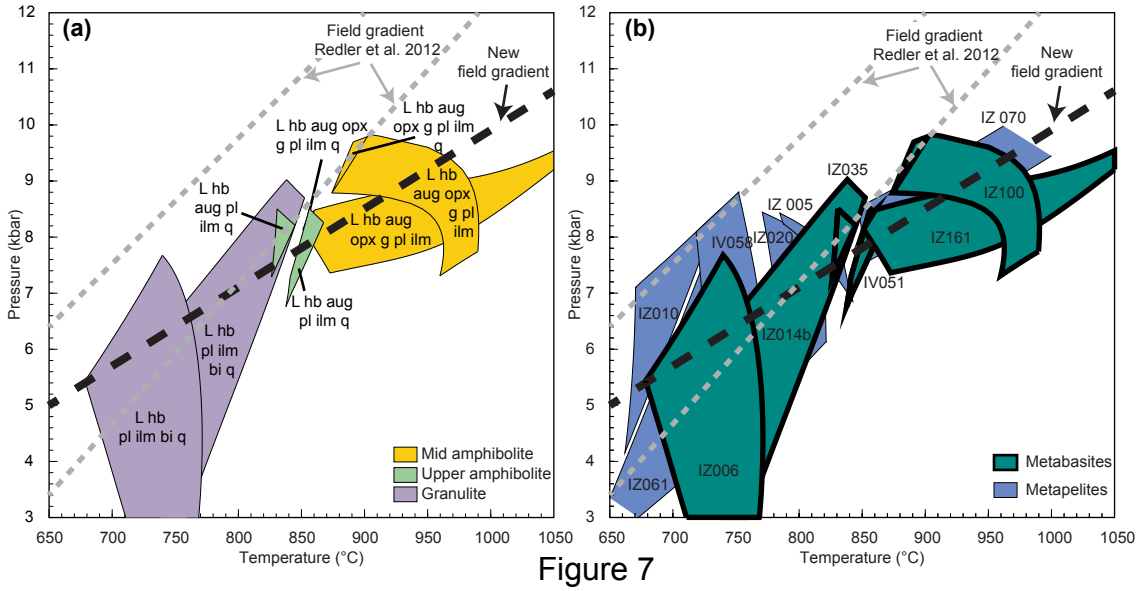

Figure 7

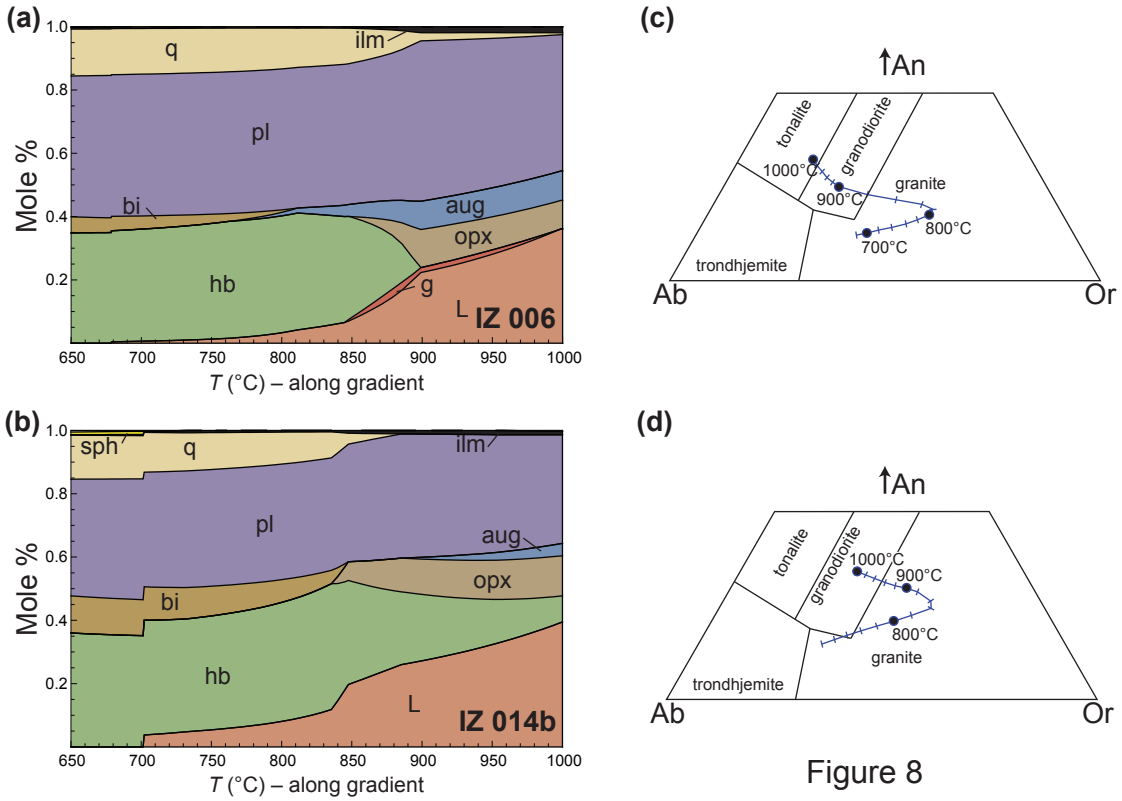

Figure 8

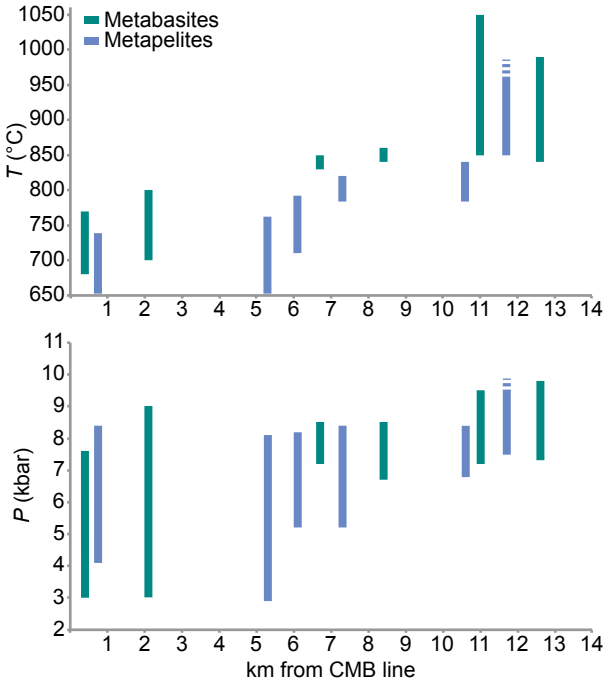

Figure 9

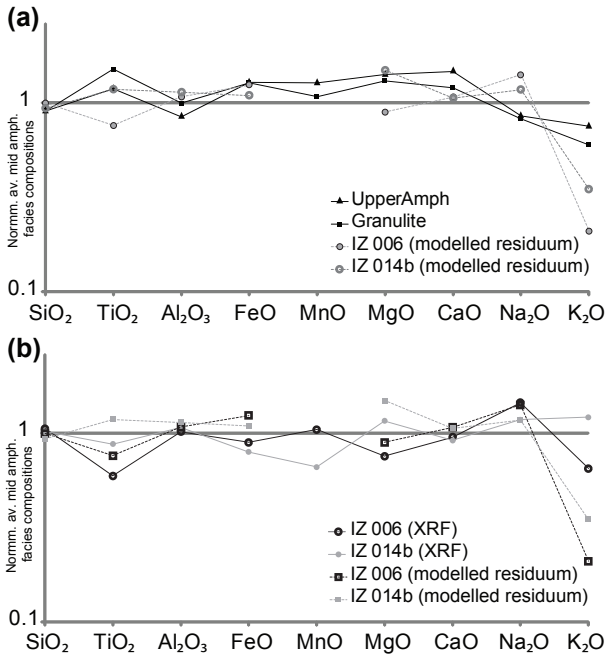

Figure 10